Trpm8 modulates thermogenesis in a sex-dependent manner without influencing cold-induced bone loss

Adriana Lelis Carvalho, PhD[1], Annika Treyball, BA[1], Daniel J. Brooks, MS[2], Samantha Costa, BS[1], Michaela R. Reagan, PhD[1,3], Mary L. Bouxsein, PhD[2], Katherine J. Motyl, PhD[1,3]*

[1]Center for Molecular Medicine, Maine Medical Center Research Institute, Scarborough, ME
[2]Center for Advanced Orthopaedic Studies, Beth Israel Deaconess Medical Center, Boston, MA
[3]Tufts University School of Medicine, Tufts University, Boston, MA

Grant Funding:
K01AR067858 to Katherine Motyl, PhD, Principal Investigator
P30GM106391 to Robert Friesel, PhD, Program Director
P30GM103392 to Don St. Germain, MD, Program Director
P20GM121301 to Lucy Liaw, PhD, Program Director
U54GM115516 to Clifford Rosen, MD, Program Director

**Address correspondence to:*
Katherine J. Motyl
81 Research Drive
Scarborough, ME 04074
(207) 396-8004
motylk@mmc.org

Figures: 6
Tables: 3
Supplementary Tables: 1
Preview link for source data (Mendeley data) doi:10.17632/3n3kg7d9np.1

Running Head: Sex differences in *Trpm8*-mediated cold acclimation

Abstract

Trpm8 (transient receptor potential cation channel, subfamily M, member 8) is expressed by sensory neurons, and it is involved in the detection of cold temperatures. Increased *Trpm8* expression triggers an increase in uncoupling protein 1 (*Ucp1*)-dependent brown adipose tissue (BAT) thermogenesis. Here, we sought to investigate whether *Trpm8* was involved in the co-regulation of thermogenesis and bone homeostasis. We exposed male and female mice with and without *Trpm8* to a 3-week cold challenge (4°C). Male *Trpm8-KO* mice exhibited a delayed cold acclimation with increased BAT expression of *Ucp1, Dio2* and *Cidea.* Conversely, female mice had no genotype-specific alterations in body temperature. Interestingly, *Trpm8* was not required for cold-induced bone loss. In summary, we identified an intriguing sex difference in the role of *Trpm8* in maintaining body temperature and composition. Furthermore, although global *Trpm8* deletion did not affect bone response to cold, it did influence cortical bone shape.

Introduction

Thermoregulatory processes involve both the regulation of heat loss and generation of heat (i.e. thermogenesis) [1]. Mammals require energy to generate and/or conserve heat when in temperatures below their thermoneutral zone, which in mice is 28-32°C [2]. During adaptation to cooler temperatures, the sympathetic nervous system (SNS) output increases, which subsequently enhances energy expenditure, fat oxidation, and heat production by brown adipose tissue (BAT). This important mechanism for maintaining body temperature homeostasis is mediated by the expression of uncoupling protein 1 (*Ucp1*) in the inner mitochondrial membrane [3,4]. In addition to non-shivering thermogenesis in BAT, cold exposure can also trigger white adipose tissue (WAT) beiging to enhance heat production. Subcutaneous WAT is more susceptible to acquiring beige adipose features compared to other WAT depots, due to its high sympathetic innervation and norepinephrine turnover rate [5]. While these functions are preserved in infants, aging leads to decreased SNS activity [6], muscle mass [7], and brown adipose mass [8] as well as impaired fatty acid oxidation, glucose tolerance, and mitochondrial biogenesis [9], leading to reduced basal metabolism, energy expenditure and impaired thermoregulatory capacity.

Aging is also associated with bone loss and higher fracture risk, which increase morbidity and mortality among the elderly population [10,11]. Interestingly, previous studies have demonstrated a relationship between SNS activity and the skeleton, revealing that sympathetic outflow is not only involved in the activation of BAT thermogenesis for thermoregulation purposes, but that sympathetic tone can also modulate bone remodeling by signaling through the β2-adrenergic receptor (β2AR) expressed by osteoblasts [12]. Motyl et al. (2013) found that altered SNS activity and impaired BAT thermogenesis were linked to trabecular bone loss in *Misty* mice, which exhibited a reduction in runt-related transcription

factor 2 (*Runx2)* expression and an increase in the transcription of the receptor activator of nuclear factor Kappa-B ligand (*Rankl*), suggesting that failure in thermoregulation mechanism can potentiate bone resorption [13]. Likewise, a more recent study has revealed that thermoneutral (32°C) housing exerted a protective effect on the skeleton, which was associated with a reduced SNS-mediated expression of the *Ucp1* in BAT [2]. Iwaniec et al. observed that an increase of 10°C in housing temperature prevented cancellous bone loss by improving bone formation and reducing bone resorption [2]. These findings indicate that the standard room temperature (22°C) housing can be considered a cold environment for a mouse and can be detrimental to the skeleton.

Transient receptor potential melastatin 8 (*Trpm8*) is a Ca^{2+} permeable, non-selective cation channel expressed by temperature-sensing sensory neurons known to be the principal detector of innocuous cold [14]. In mice, *Trpm8* is activated by a wide temperature range, approximately between 28°C to 8°C, and also by cooling agents (e.g. menthol and icilin) [15]. Previously, *Trpm8* was primarily described to work as a peripheral thermal sensor; however, there is evidence that this cold-sensing channel is also involved in thermoregulation by promoting heat conservation and energy homeostasis [1]. Indeed, *Trpm8* is considered as a potential target in obesity due to its function in regulating energy metabolism [1,16–20]. *Trpm8* has been found to trigger non-shivering thermogenesis by BAT and the beiging of WAT in mice [20] and humans [18]. Moreover, *Trpm8* knockout (Trpm8-KO) mice presented features such as hyperphagia and reduced fat oxidation when housed at 21°C, which seemed to promote the development of obesity [1].

Human osteoblast-like cells and murine osteoblast cells can also express *Trpm8,* which indicates it can potentially directly impact bone [21]. Although the deletion of other *Trp* channels, such as *Trpv1* [22] and *Trpv5* [23], has been reported to induce bone loss in animal models, there

is a lack of data exploring the physiological role of *Trpm8* in skeletal homeostasis. We hypothesized that *Trpm8* deletion could lead to more severe bone loss with cold challenge due to poor body temperature regulation. Therefore, we sought to investigate whether *Trpm8* is involved in the co-regulation of BAT and bone tissues by exposing one-year-old male and female WT and *Trpm8* knockout (KO) mice to a cold housing (4°C) treatment. Importantly, we tested whether bone and adipose tissue changes are different in males and females, since women have higher fracture risk with age.

Materials and Methods

Wild-type (WT) and *Trpm8-knockout* (*Trpm8-KO*) mice were purchased from The Jackson Laboratory (stock #008198). Mice were bred and housed in a barrier animal facility at Maine Medical Center Research Institute (MMCRI) on a 14-hr light and 10-hr dark cycle. Mice were aged to 52 weeks while being housed up to four animals per cage at 22°C. Mice were given water and regular chow *ad libitum*. The study was approved by the Institutional Animal Care and Use Committee (IACUC) of MMCRI (approval number 1017). Euthanasia was performed using isoflurane followed by cervical dislocation or decapitation.

Cold exposure Study

Fifty-two week-old WT and *Trpm8-KO* mice were separated into individual cages. Half of the mice were maintained at room temperature, while the other half were moved to a cold room. Cold-treated mice were exposed to 18°C for 1 week, then 4°C for 3 weeks. Rectal temperature was measured daily and every 2 hours on the day of change to 4°C. Cages contained standard bedding, regular chow and water *ad libitum.*

Dual-energy X-ray absorptiometry (DXA)

All mice had body weight measured prior to DXA measurement. Bone mineral content (aBMC), bone mineral density (aBMD), lean mass and fat mass measurements were performed on each mouse by a PIXImus dual energy X-ray densitometer (GE Lunar, GE Healthcare). The PIXImus was calibrated daily with a mouse phantom provided by the manufacturer. Mice were ventral side down with each limb and tail positioned away from the body. Full-body scans were obtained, and the head was excluded from analyses because of concentrated mineral content in skull and teeth. X-ray absorptiometry data were processed and analyzed with Lunar PIXImus 2 (version 2.1) software [24]. Adiposity index was defined as fat mass divided by fat-free mass.

Histology

Femur and all adipose tissue samples were placed in 10% neutral buffered formalin (Sigma-Aldrich) for 48 hr and then kept in 70% ethanol. Tissues sections of 5 μm were deparaffinized and dehydrated in a graded series (100-70%) of ethanol washes and stained with hematoxylin and eosin (H&E). Pictures from H&E stained femur at 4x magnification were taken to evaluate adipocytes content in the bone marrow.

Bone Marrow Adipocyte Quantification and Analysis

A blinded analysis of bone marrow (BM) adipocytes was performed on each histology slide using ImageJ software (https://imagej.nih.gov/ij/) [25,26]. A global scale was set at 1000 pixels/mm based on the microscope imaging objective and settings. The tissue area (T.Ar) was selected in the distal femoral metaphysis (0.1 mm below the epiphyseal growth plate) using the polygon tool to contain the BM, excluding cortical bone. One histological slide per distal femur was measured. The T.Ar was measured using ImageJ to find the total tissue area, which was used to normalize adipocyte numbers per T.Ar for each image. Color images were converted to 32-bit and then thresholded using the *Huang* filter at the automatic level determined by ImageJ [25,26]. [Note: thresholding an image converts it to black (255) and white (0) values [25,26].

Images were then processed with the *Despeckle* and *Adjustable Watershed* plugins. [*Despeckle* was used to automatically remove salt-and-pepper background noise that could cause inaccuracies with particle analysis, while the *Adjustable Watershed* ImageJ segmentation algorithm was used to systematically correct any adjacent adipocytes that had been merged into 1, back into 2 distinct objects. ImageJ typically applies a watershed segmentation threshold at a level of 0.5, but with the *Adjustable Watershed* the amount of segmentation can be changed to correct for closely packed adipocyte, tissue tears, or staining inconsistencies [25,26]. A blinded investigator set the *Adjustable Watershed* within the range of 0.3-0.8 to select the most appropriate segmentation threshold to apply to each image based solely on the quality of the individual image. Next, particle analysis for BM adipocytes was performed within the T.Ar using the *Analyze Particles* plugin. This plugin scans a selected area and measures objects that meet parameters based on area and circularity [25,26]. The particle circumference range was set to 50-2500 pixels (area results displayed in mm^2 due to the set global scale) and the circularity was set at 0.60-1.00 (1.00 being a perfect circle). These parameters were determined through an iterative, trial and error analysis of different images until a universal measurement system was decided upon and then used for every image. After particle analysis, the *Result* and *Summary* pop-up windows provided the individual and average area (mm^2) for each counted adipocyte within the T.Ar; these data were used to quantify adiposity in each sample (based on adipocyte number and average adipocyte area).

Micro-computed tomography (µCT)

A high-resolution desktop micro-tomographic imaging system (µCT40, Scanco Medical AG, Brüttisellen, Switzerland) was used to assess trabecular bone architecture in the distal femoral metaphysis and L5 vertebral body and cortical bone morphology of the femoral mid-diaphysis. Scans were acquired using a 10 μm^3 isotropic voxel size, 70 kVP, 114 µA, 200 ms integration time, and were subjected to Gaussian filtration and segmentation. Image acquisition

and analysis protocols adhered to guidelines for the assessment of rodent bones by μCT [27]. In the femur, trabecular bone microarchitecture was evaluated in a 1500 μm (150 transverse slices) region beginning 200 μm superior to the peak of the growth plate and extending proximally. In the L5 vertebral body, trabecular bone was evaluated in a region beginning 100 μm inferior to the cranial end-plate and extending to 100 μm superior to the caudal end-plate. The trabecular bone regions were identified by manually contouring the endocortical region of the bone. Thresholds of 335 mgHA/cm^3 and 385 mgHA/cm^3 were used to segment bone from soft tissue in the femur and L5 vertebrae, respectively. The following architectural parameters were measured using the Scanco Trabecular Bone Morphometry evaluation script: trabecular bone volume fraction (Tb.BV/TV, %), t rabecular bone mineral density (Tb. BMD, mgHA/cm^3), specific bone surface (BS/BV, mm^2/mm^3), trabecular thickness (Tb.Th, mm), trabecular number (Tb.N, mm^{-1}), and trabecular separation (Tb.Sp, mm), connectivity density (Conn.D, 1/mm^3). Cortical bone was assessed in 50 transverse μCT slices (500 μm long region) at the femoral mid-diaphysis and the region included the entire outer most edge of the cortex. Cortical bone was segmented using a fixed threshold of 708 mgHA/cm^3. The following variables were computed: total cross-sectional area (bone + medullary area) (Tt.Ar, mm^2), cortical bone area (Ct.Ar, mm^2), medullary area (Ma.Ar, mm^2), bone area fraction (Ct.Ar/Tt.Ar, %), cortical tissue mineral density (Ct.TMD, mgHA/cm^3), cortical thickness (Ct.Th, mm), cortical porosity (%), as well as bone strength indicators such as maximum, minimum and polar moments of inertia (I_{max}, I_{min}, and pMOI, mm^4), which describe the shape/distribution of cortical bone (larger values indicate a higher bending strength). Cortical bone images were taken of the mouse using the median total area value within each group. The scale for all of the images is 1 mm equals 315 pixels.

Real-time PCR

Adipose tissues (brown and gonadal adipose tissue) and tibias were collected from 56 week-old WT and *Trpm8-KO* mice for RNA extraction under liquid nitrogen conditions. Total RNA was prepared using the standard TRIzol (Sigma-Aldrich) method for tissues. cDNA was generated using the High Capacity cDNA Reverse Transcriptase Kit (Applied Biosystems) according to the manufacturer's instructions. mRNA expression analyses was carried out using an iQ SYBR Green Supermix with a BioRad® Laboratories CFX Connect Real-time System thermal cycler and detection system. TATA binding protein 1 (Tbp1) was used as an internal standard control gene for all quantification [28]. Primers used were from Integrated DNA Tecnologies (IDT) (Coralvile, IA) [29–31]and Primer Design (Southampton, UK). All primer sequences are listed in Supplementary Table I.

Supplemental Table I. qPCR primer information.

Target Gene	Source/Supplier	Sequence	Reference
Acadl	Primer Design (Southampton, UK)	Forward: 5'-GGA ATG AAA GCT CAG GAC ACA -3' Reverse: 5'-AGC CTT TAT TCT CTT CTC CAA GT -3'	NA
Cidea	IDT (Coralvile, IA)	Forward: 5'-TGC TCT TCT GTA TCG CCC AGT -3' Reverse: 5'-GCC GTG TTA AGG AAT CTG CTG -3'	Seale et al. (2008)
Dio2	IDT (Coralvile, IA)	Forward: 5'-CAG TGT GGT GCA CGT CTC CAA TC -3' Reverse: 5'-TGA ACC AAA GTT GAC CAC CAG -3'	Cooper et al. (2008)
Pdk4	Primer Design (Southampton, UK)	Forward: 5'-AAA GTG GGT CTG TGG CAT TG -3' Reverse: 5'-AAG GTT TGT ACT CGT GTT TGT G -3'	NA
Pparc1α	IDT (Coralvile, IA)	Forward: 5'- TGA TGT GAA TGA CTT GGA TAC AGA CA -3' Reverse: 5'- GCT CAT TGT TGT ACT GGT TGG ATA TG -3'	Cooper et al. (2008)
Pparγ2	IDT (Coralvile, IA)	Forward: 5'-GCA TGG TGC CTT CGC TGA -3' Reverse: 5'-TGG CAT CTC TGT GTC AAC CAT G -3'	Cooper et al. (2008)
Prdm16	IDT (Coralvile, IA)	Forward: 5'-CAG CAC GGT GAA GCC ATT C -3' Reserve: 5'-GCG TGC ATC CGC TTG TG -3'	Cooper et al. (2008)
Tbp1	IDT (Coralvile, IA)	Forward: 5'-GAA GCT GCG GTA CAA TTC CAG -3' Reserve: 5'-CCC CTT GTA CCC TTC ACC AAT -3'	Sanchez-Gurmaches and Guertin (2014)
Ucp1	IDT (Coralvile, IA)	Forward: 5'-ACT GCC ACA CCT CCA GTC ATT-3' Reverse: 5'- CTT TGC CTC ACT CAG GAT TGG -3'	Cooper et al. (2008)

Statistical analysis

GraphPad Prism 8® software was used to perform statistical tests. Data are presented as mean ± standard error. Student's t test or two-way ANOVA was performed with Holm-Sidak *post doc* multiple comparison test as needed. $\alpha \leq 0.05$ was considered statistically significant.

Results

Male Trpm8-KO mice had a lower core temperature, body weight and bone mineral density than WT mice

Core temperature (n=7 to 11/group), body composition and bone density (n=14-19/group) were assessed at baseline (52 weeks of age) at standard room temperature (22°C). Male *Trpm8-KO* mice had a lower core temperature (-0.7°C; p=0.02) compared to male WT mice. Male *Trpm8-KO* mice also had reduced body mass compared to male WT mice, which was associated with lower fat and lean mass as well as reduced total areal bone mineral density (aBMD) and areal bone mineral content (aBMC) measures (Table I). On the other hand, female *Trpm8-KO* mice had no difference in core temperature compared to female WT mice. However, reduced body mass was also observed in female *Trpm8-KO* mice compared to female WT group due to lower fat mass. Female *Trpm8-KO* mice had no difference in lean mass, aBMC and aBMD measurements compared to female WT mice (Table I).

Table I. Core temperature measures and body composition and bone outcomes assessed by DXA of *Wild-type* (WT) and *Trpm8-Knockout* (*KO*) at baseline.

Variables (baseline) RT=22°C	**Male** (52 week-old)		**Female** (52 week-old)	
	***Wild-type* (WT)** (mean ± SEM)	***Trpm8-KO*** (mean ± SEM)	***Wild-type* (WT)** (mean ± SEM)	***Trpm8-KO*** (mean ± SEM)
Core temperature (°C)	37.71 ± 0.46	37.01 ± 0.53 *	37.08 ± 0.62	36.75 ± 0.60
Body composition				
Body Mass (g)	47.0 ± 0.8	41.0 ± 2.0 *	35.7 ± 1.1	32.1 ± 1.2 *
Fat Mass (g)	17.0 ± 0.9	13.0 ± 1.2 *	14.1 ± 1.0	10.9 ± 1.0 *
Fat-Free Mass (g)	30.0 ± 0.9	27.0 ± 0.7 *	20.4 ± 0.4	20.1 ± 0.4
Adiposity Index	0.57 ± 0.04	0.48 ± 0.04	0.69 ± 0.05	0.54 ± 0.04 *
Bone mineral density (BMD)				
Femur aBMD (g/cm^2)	0.076 ± 0.001	0.075 ± 0.001	0.069 ± 0.002	0.067 ± 0.001
Femur aBMC (g)	0.0106 ± 0.0002	0.0103 ± 0.0001	0.0096 ± 0.0002	0.0092 ± 0.0002
Total aBMD (g/cm^2)	0.0543 ± 0.0007	0.0519 ± 0.0004 *	0.0516 ±0.0005	0.0509 ± 0.0004
Total aBMC (g)	0.585 ± 0.011	0.513 ± 0.007 ***	0.471 ± 0.010	0.455 ± 0.010

*p<0.05 and ***p<0.0001 compared to WT mice. SEM = standard error of mean. Number of mice: male = 13 to 21 and female = 14 to 21. aBMD = areal bone mineral density; aBMC = areal bone mineral content.

The ability to adapt to a cold environment is Trpm8 and sex-dependent

Fifty-two week-old male and female WT and *Trpm8-KO* mice were individually housed either at room temperature (22°C) or at cold temperature (4°C) for 4 weeks (Figure 1A). Male and female WT and *Trpm8-KO* cold-housed mice were gradually exposed to colder housing temperatures, initially spending 1 week at 18°C before being placed at 4°C for 3 weeks (Figure 1A). We observed that male *Trpm8-KO* mice exhibited significant lower core temperature than male WT mice at 22°C at baseline ($p=0.0065$); this difference persisted after 1 week housed at 18°C ($p=0.02$) (Figure 1B).

Figure 1. Absence of *Trpm8* cold-sensing channel induced delayed temperature acclimation in male mice. (A) Long-term cold study experimental design illustrating that male and female mice were individually housed at standard room temperature (RT) (22°C) or cold temperature (4°C) during the study period. All mice from the cold housing group were acclimated at 18°C for one week prior to being housed at 4°C for 3 weeks. (B) Core temperature measurements from male and female WT and *Trpm8-KO* mice throughout the study. (C) Core temperature measurements from male and female WT and *Trpm8-KO* during the first 8 hours of mice being housed at 4°C.

In week 2, in the first 8 hours after being moved to 4°C housing, male *Trpm8-KO* mice were able to maintain their initial core temperature compared to WT mice, but only for the first 4 hours (Figure 1C). After that, we observed that male WT mice demonstrated a significant increase in their core temperature between 2 and 4 hours at 4°C (Figure 1C). On the other hand, we found that, between 4 to 8 hours at 4°C, core temperature of *Trpm8-KO* mice was significant lower compared to WT mice ($p<0.05$) (Figure 1C). However, by the end of week 2, male *Trpm8-KO* mice had acclimated to the cold exposure and reached core temperatures similar to those of male WT mice ($p=0.06$), which was maintained until the endpoint of the study (Figure 1B).

Conversely, there were no differences between female WT and *Trpm8-KO* mice at room temperature. WT and *Trpm8-KO* mice responded similarly to 18°C and 4°C cold challenge (Figure 1B). Core temperature was similar between female WT and *Trpm8-KO* mice during the first 8 hours of 4°C cold exposure (Figure 1C) and throughout the 3 weeks of cold housing (Figure 1B).

Body weight reduction was associated with changes in adipose tissue profile in response to cold exposure

Male mice exposed to cold housing for 3 weeks lost weight, irrespective of genotype (Figure 2A). Cold exposure induced BAT expansion in male WT and *Trpm8-KO* mice ($p<0.05$) (Figure 2B). Gonadal WAT (gWAT) mass was reduced only in male WT mice ($p=0.046$) after 3 weeks of cold exposure whereas no significant effect on inguinal WAT (iWAT) was observed at the endpoint, regardless of mouse genotype (Figure 2B). Female WT and *Trpm8-KO* mice also lost weight after being exposed to cold housing for 3 weeks (Figure 2C). However, unlike males, the expansion of BAT mass in female mice was observed only in the WT group ($p=0.002$) in response to cold, but not in female *Trpm8-KO* mice (Figure 2D). Moreover, gWAT mass was reduced only in female *Trpm8-KO* mice ($p=0.02$) with cold exposure, and there was also no change in iWAT mass at the endpoint, regardless of the mouse genotype (Figure 2D).

Figure 2. Cold exposure led to body weight loss, BAT expansion, and gWAT loss. (A) Body weight assessment from male WT and *Trpm8-KO* mice housed at standard room temperature (RT) (22°C) and cold temperature (4°C) at baseline and endpoint. (B) Fat pad weights from male WT and *Trpm8-KO* housed at 22°C and 4°C at the baseline and endpoint. (C) Body weight assessment from female WT and *Trpm8-KO* housed at 22°C and 4°C at baseline and endpoint. (D) Fat pad weights from female WT and *Trpm8-KO* housed at 22°C and 4°C at baseline and endpoint. (E and F) Representative H&E stained image of BAT from male

and female WT and *Trpm8-KO* housed at 22°C and 4°C. (G and H) Representative H&E stained image of gWAT from male and female WT and *Trpm8-KO* housed at 22°C and 4°C (scale bar: 100 μm; magnification: 20x). Data presented as mean ± standard error. *p<0.05 and **p<0.01 by Holm-Sidak *post doc* test after a significant two-way ANOVA.

These outcomes are consistent with H&E stained BAT (Figures 2E and F) and histological images of gWAT from male and female WT and *Trpm8-KO* mice housed at room temperature or cold (Figures 2G and H). Specifically, we observed larger lipid droplets in BAT from male mice of both genotypes at room temperature compared to females. After cold exposure, lipid droplets were smaller in BAT from both genotypes and sexes, indicative of more active thermogenesis (Figures 2E and F). However, the difference in BAT lipid droplets between room temperature and cold cohorts appeared more striking in males compared to females of both genotypes (Figures 2E and F). In gWAT, the adipocyte size appeared similar between genotypes, but larger in males than in females (Figures 2G and H). Cold exposure reduced adipocyte size in both genotypes and sexes, but most dramatically in female mice (Figure 2H).

Delayed temperature acclimation in male Trpm8-KO mice preceded increased fatty acid metabolism markers in BAT and increased Ucp1 in gWAT.

In male *Trpm8-KO* mice, we found numerous changes in the BAT expression of fatty acid metabolism and thermogenic markers after cold challenge. We found that BAT expression of fatty acid metabolism markers such as *Acadl* (p=0.004), *Prdm16* (p=0.0059), and *Pparc1α* (p=0.0079) were higher in male *Trpm8-KO* mice compared to male WT mice following 3 weeks of being housed at 4°C (Figure 3A). Moreover, *Acadl* expression was also higher in male *Trpm8-KO* housed at 4°C compared to *Trpm8-KO* mice housed at 22°C (p=0.027) (Figure 3A). However, there were no changes in the expression of *Pparγ2 and Pdk4* among groups. As expected, BAT expression of *Ucp1* was higher in male WT mice housed at 4°C compared to

those at 22°C (p=0.012) (Figure 3A). Interestingly, male *Trpm8*-KO mice housed at 4°C had equivalent levels of *Ucp1* expression compared to WT at 4° C. However, *Ucp1* expression in BAT was not significantly elevated in male *Trpm8*-KO mice housed at 4°C compared to *Trpm8-KO* at 22°C due to variability in this outcome at room temperature (Figure 3A). However, they did respond with increased BAT expression of other thermogenic markers, such as *Cidea* (p=0.006) *and Dio2* (p=0.0051)*,* which were expressed at higher levels in cold-treated male *Trpm8*-KO mice than their room temperature (p<0.05) and WT (p<0.0001) counterparts (Figure 3A). These findings suggest that, in male mice, cold exposure stimulated the expression of both fatty acid oxidation and thermogenesis markers within BAT in the absence of *Trpm8* which seemed to be sufficiently for them to eventually achieve optimal body temperature.

Figure 3. Cold promotes expression of fatty acid metabolism and thermogenic markers in BAT of *Trpm8-KO males*. (A) Fatty acid metabolism (*Acadl, Prdm16, Pparc1α, Pparγ2, and Pdk4*) and thermogenic (*Ucp1, Cidea, and Dio2*) marker expression in the BAT of male WT and *Trpm8-KO* mice housed at standard room temperature (RT) (22°C) and cold temperature (4°C) (n=5-6). (B) Fatty acid metabolism and thermogenic marker expression in the gWAT of male WT and *Trpm8-KO* housed at 22°C and 4°C (n= 4-7). Data presented as mean ± standard error. *p<0.05; **p<0.01; and ***p<0.0001 by Holm-Sidak *post doc* test after a significant two-way ANOVA. For primers sequence see also Supplemental Table I.

Unlike in BAT, we did not observe significant changes in gWAT expression of the fatty acid metabolism markers (*Acadl*, *Pparc1α,* and *Pparγ2*) (Figure 3B). Instead, we found that *Prdm16*, a transcription factor involved in the differentiation of progenitor cells into brown adipocytes, was reduced in male *Trpm8-KO* mice (p=0.013) compared to male WT mice housed at 22°C (Figure 3B). Cold temperature had no significant effect on *Prdm16* expression in the gWAT of male *Trpm8-KO* mice (Figure 3B). Likewise, *Pdk4*, a fatty acid oxidation marker, had reduced expression in gWAT of male WT mice housed at 4°C compared to those WT mice housed at 22°C (p=0.02), but no difference related to the mouse genotype was found (Figure

3B). In these findings, there is no evidence of beiging in gWAT associated with cold challenge or genotype. A wide variation in *Ucp1* expression in gWAT was observed in cold-treated WT and *Trpm8-KO* groups. However, we found that cold exposure led to an increase in gWAT expression of *Ucp1* in male *Trpm8-KO* mice (p=0.03) compared to those housed at 22°C, a significant effect that was not observed in the corresponding WT groups (Figure 3B). However, there was no significant difference in the expression of other thermogenic markers (*Cidea* and *Dio2*) in gWAT (Figure 3B). These findings suggest that some thermogenesis may also arise from this depot upon cold challenge, but it does not seem to be related to *Trpm8* deletion.

Gonadal white adipose tissue (gWAT) plays a major role in sustaining body temperature in female mice independent of Trpm8 deletion

In female mice, the expression of fatty acid metabolism markers such as *Acadl*, *Prdm16, Pparc1α,* and *Pdk4* in BAT was similar between WT and *Trpm8-KO* mice (Figure 4A), with the exception being *Pparγ2*. Expression of *Pparγ2* was lower in BAT of female mice housed at 4°C compared to those housed at 22°C, regardless of the genotype (WT: p=0.013; *Trpm8-KO*: p=0.0086) (Figure 4A). In female *Trpm8*-KO mice, cold exposure induced an increase in BAT expression of *Ucp1* compared to room temperature (p=0.048) (Figure 4A), but there was no significant upregulation of *Ucp1* in female WT mice due to variability of the expression within the group. Unlike in male mice, expression other thermogenic markers (*Cidea* or *Dio2*) were unaltered in BAT of female mice (Figure 4A). Overall, these results indicate maintenance of body temperature after cold exposure induces *Ucp1* expression in female *Trpm8-KO* mice to a greater extent than in WT, but most other markers for thermogenesis-related processes were equivalently expressed.

Figure 4. Cold-induced expression of thermogenic and fatty acid metabolism in females independently of *Trpm8.* (A) Fatty acid metabolism (*Acadl, Prdm16, Pparc1α, Pparγ2, and*

Pdk4) and thermogenic (*Ucp1, Cidea, and Dio2*) marker expression in the BAT of female WT and *Trpm8-KO* mice housed at standard room temperature (RT) (22°C) and cold temperature (4°C) (n= 6). (B) Fatty acid metabolism and thermogenic marker expression in gWAT of female WT and *Trpm8-KO* housed at 22°C and 4°C (n=4-7). Data presented as mean ± standard error. *p<0.05; **p<0.01; and ***p<0.0001 by Holm-Sidak *post doc* test after a significant two-way ANOVA. For primers sequence see also Supplemental Table I.

Female mice exhibited changes in the gWAT expression of fatty acid metabolism markers (*Acadl*, *Pparc1α,* and *Pdk4*), after 3 weeks of cold exposure (Figure 4B). Both female WT and *Trpm8-KO* mice housed at 4°C demonstrated an increase in *Acadl* and *Pparc1α* expression compared to female mice housed at 22°C (p<0.05) (Figure 4B). However, a higher *Pdk4* expression in gWAT was only observed between female WT mice housed at 4°C compared to those housed at 22°C (p<0.05) (Figure 4B). In addition, unlike in male mice, cold exposure induced the expression of thermogenic markers (*Ucp1, Cidea* and *Dio2)* in the gWAT of females. In fact, we found an increase in the expression of *Ucp1* and *Dio2* expression in gWAT in female mice, irrespective of genotype (p<0.05) (Figure 4B). *Ucp1* expression in gWAT was particularly highly expressed in female WT mice housed at 4°C compared to those housed at 22°C (p<0.0001) (Figure 4B). These data suggest that gWAT is a major contributor to heat production and body thermoregulation in females with and without the *Trpm8* deletion when exposed to a colder environment. This is in contrast to males, where gWAT may play less of a role.

Trpm8 deletion is associated with reduced femur length and altered cortical structure in male mice irrespective of housing temperature

Because altered thermogenesis has previously been associated with changes in bone homeostasis [13], we next examined bone microarchitectural phenotypes of WT and *Trpm8-KO*

mice at room temperature and with cold exposure. Femur length was significantly reduced in male *Trpm8-KO* mice compared to male WT mice (p=0.01), but this was not altered by temperature. The minimum moment of inertia (I*min*) was lower in male *Trpm8-KO* mice compared to male WT mice in both housing temperatures (22°C: p=0.03 and 4°C: p=0.024) (Table II). *Trpm8* deletion also decreased other femoral bone parameters such as marrow area (Ma.Ar), total cross-sectional area (Tt.Ar), and polar moment of inertia (pMOI) (*p*=0.01), but pairwise comparisons were not statistically significant (Table II and Figure 5A).

Figure 5. Female *Trpm8-KO* mice may have a temperature-independent impact in bone marrow adipose tissue (BMAT). (A and B) Representative µCT images of cortical bone from male and female WT and *Trpm8-KO* mice housed at standard room temperature (RT) (22°C) and cold temperature (4°C). (C and D) Quantification of adipocyte numbers (Ad.N/T.Ar), average adipocyte size (Ad.A), and % adiposity (T.Ar Adiposity) within the bone marrow of male and female WT and *Trpm8-KO* mice housed at 22°C and 4°C. (E and F) Representative H&E stained image of distal femur area from male and female WT and *Trpm8-KO* mice housed at 22°C and 4°C (scale bar: 500 µm; magnification: 4x). Data presented as mean ± standard error.

Table II. Femoral and Vertebral Bone outcomes assessed by µCT of Male *Wild-type* (WT) and *Trpm8-Knockout* (*KO*) mice after 3 weeks of study.

Variables	**Male** (56 week-old)				**P value**		
	Room temperature housing (22°C)		**Cold housing (4°C)**				
	***Wild-type* (WT)** (mean ± SEM)	***Trpm8-KO*** (mean ± SEM)	***Wild-type* (WT)** (mean ± SEM)	***Trpm8-KO*** (mean ± SEM)	***Source of variation***		
Femoral bone outcomes					***genotype***	***temperature***	***interaction***
Femur length (mm)	15.57 ± 0.06	15.07 ± 0.13 *	15.42 ± 0.14	15.26 ± 0.16	**0.01**	0.88	0.19
BV/TV (%)	11.06 ± 0.83	11.85 ± 0.93	8.87 ± 1.01	9.89 ± 1.10	0.36	**0.04**	0.91
Conn.D (1/mm^3)	42.61 ± 6.62	58.51 ± 8.95	31.23 ± 5.79	43.14 ± 7.28	0.07	0.08	0.79
Tb.N (1/mm)	3.014 ± 0.133	3.154 ± 0.073	2.782 ± 0.055	3.006 ± 0.098	0.07	0.06	0.67
Tb.Th (mm)	0.059 ± 0.001	0.061 ± 0.003	0.058 ± 0.002	0.056 ± 0.002	0.95	0.15	0.19
Tb.Sp (mm)	0.323 ± 0.017	0.304 ± 0.007	0.347 ± 0.007	0.321 ± 0.011	0.07	0.09	0.78
Ct.Th (mm)	0.159 ± 0.007	0.161 ± 0.008	0.160 ± 0.006	0.154 ± 0.004	0.20	0.67	0.52
Ct.Ar (mm^2)	0.879 ± 0.038	0.861 ± 0.040	0.877 ± 0.026	0.816 ± 0.026	0.26	0.49	0.52
Ct.TMD (mgHA/cm^3)	1195.34 ± 6.71	1197.48 ± 5.02	1197.93 ± 8.06	1191.52 ± 5.09	0.73	0.79	0.50
Ma.Ar (mm^2)	1.766 ± 0.098	1.520 ± 0.051	1.743 ± 0.108	1.537 ± 0.060	**0.01**	0.97	0.81
Tt.Ar (mm^2)	2.644 ± 0.088	2.381 ± 0.059	2.620 ± 0.116	2.356 ± 0.074	**0.005**	0.77	0.99
Ct.Ar/Tt.Ar (%)	33.51 ± 1.87	36.23 ± 1.51	33.70 ± 1.43	34.77 ± 0.87	0.21	0.67	0.58
Ct. Porosity (%)	0.23 ± 0.03	0.26 ± 0.03	0.20 ± 0.01	0.23 ± 0.02	0.27	0.14	0.87
pMOI (mm^4)	0.643 ± 0.038	0.576 ± 0.035	0.638 ± 0.042	0.544 ± 0.033	**0.04**	0.63	0.72
Imax (mm^4)	0.424 ± 0.029	0.399 ± 0.026	0.418 ± 0.029	0.369 ± 0.027	0.19	0.53	0.67
Imin (mm^4)	0.219 ± 0.011	0.177 ± 0.010 *	0.222 ± 0.016	0.177 ± 0.009 *	**0.0009**	0.89	0.89
Vertebral bone outcomes					***genotype***	***temperature***	***interaction***

BV/TV (%)	21.61 ± 1.10	20.67 ± 1.75	18.72 ± 0.53	18.42 ± 0.67	0.59	**0.04**	0.78
BS/BV (mm^2/mm^3)	43.920 ± 1.482	44.476 ± 1.859	46.177 ± 0.356	46.873 ± 0.321	0.62	0.08	0.95
BMD ($mgHA/cm^3$)	226.43 ± 9.98	217.29 ± 16.16	198.17 ± 4.74	197.57 ± 5.90	0.65	**0.03**	0.69
Conn.D ($1/mm^3$)	127.37 ± 11.45	115.30 ± 7.95	112.82 ± 5.25	118.71 ± 8.43	0.73	0.53	0.32
Tb.N (1/mm)	4.426 ± 0.135	4.307 ± 0.148	4.092 ± 0.079	4.190 ± 0.146	0.94	0.11	0.43
Tb.Th (mm)	0.050 ± 0.001	0.053 ± 0.002	0.050 ± 0.003	0.053 ± 0.002	0.10	0.96	0.96
Tb.Sp (mm)	0.215 ± 0.007	0.223 ± 0.009	0.236 ± 0.005	0.230 ± 0.009	0.89	0.08	0.37

*$p<0.05$ compared to WT mice group. Number of mice/group = 6 – 7 mice. BV/TV = bone volume fraction; Conn.D = connectivity density; Tb.N = trabecular number; Tb.Th = trabecular thickness; Tb.Sp = trabecular separation; Ct.Th = average cortical thickness; Ct.Ar = cortical bone area; Ct.TMD = cortical tissue mineral density; M.Ar = marrow area; T.Ar = total cross-sectional area; Ct.Ar/T.Ar = cortical area fraction; Ct.Porosity = cortical porosity; pMOI = polar moment of inertia; Imax = maximum moment of inertia; Imin = minimum moment of inertia; BMD = bone mineral density; BS/BV =specific bone surface.

Cold exposure was associated with lower trabecular bone volume fraction (BV/TV) at both skeletal sites evaluated (p=0.04), and reduced vertebral bone mineral density (BMD) (p=0.03), irrespective of the genotype; however, these did not reach statistical significance after multiple comparison test (Table II). We also evaluated whether cold exposure and/or genotype would affect the number of adipocytes (Ad.N/T.Ar), average adipose size (average Ad.A), and the percent of adiposity per total area (T.Ar Adiposity) within bone marrow. In general, bone marrow adipose tissue (BMAT) is limited in male mice compared to females. Here, we found that neither cold exposure nor *Trpm8* deletion had any effect on BMAT in males (Figure 5C and E). However, we found a significant interaction between genotype and housing temperature (p=0.045) suggesting that male *Trpm8-KO* mice have greater percent of adiposity when housed at 4°C, but pairwise comparisons were not statistically significant.

Female Trpm8-KO mice had impaired cortical bone regardless of housing temperature

Female *Trpm8-KO* mice are more disposed to have reduced cortical bone area (Ct.Ar), total cross-sectional area (Tt.Ar) and reduced indicators of strength, such as polar moment of inertia (pMOI), maximum moment of inertia (I_{max}), and minimum moment of inertia (I_{min}) compared to female WT mice (Table III and Figure 5B). Moreover, we found that female *Trpm8-KO* mice exhibited reduced vertebral trabecular bone volume (BV/TV), bone mineral density (BMD), trabecular number (Tb.N), and increased trabecular separation compared to female WT mice. However, cold challenge had no further impact on those bone parameters. Instead, cold exposure increased cross-sectional marrow area (Ma.Ar) and reduced cortical area fraction (Ct.Ar/T.Ar) by the endpoint of the study. Cold challenge also induced increases in vertebral specific bone surface (BS/BV), but there were no differences between genotypes in these variables after multiple comparison tests (Table III and Figure 5B). Interestingly, we found that in

females, absence of *Trpm8* had the significant main effects of reduced number of adipocytes within the marrow (Ad.N/T.Ar) ($p=0.0052$) and % of adiposity per total area (T.Ar Adiposity) ($p=0.02$). However, after multiple comparisons test, there were no statistical differences between individual groups (Figure 5D and F). We also did not observe any effect of temperature on BMAT (Figure 5D and F).

Table III. Femoral and Vertebral Bone outcomes assessed by µCT of Female *Wild-type* (WT) and *Trpm8-Knockout* (*KO*) mice after 3 weeks of study.

Variables	**Female** (56 week-old)				P value		
	Room temperature housing (22°C)		**Cold housing (4°C)**				
	***Wild-type* (WT)** (mean ± SEM)	***Trpm8-KO*** (mean ± SEM)	***Wild-type* (WT)** (mean ± SEM)	***Trpm8-KO*** (mean ± SEM)	***Source of variation***		
Femoral bone outcomes					***genotype***	***temperature***	***interaction***
Femur length (mm)	15.50 ± 0.18	15.34 ± 0.15	15.58 ± 0.05	15.51 ± 0.11	0.37	0.31	0.73
BV/TV (%)	2.130 ± 0.384	2.782 ± 0.902	1.874 ± 0.196	2.575 ± 0.781	0.32	0.73	0.97
Conn.D (1/mm^3)	4.331 ± 1.392	14.382 ± 7.938	6.569 ± 1.667	15.905 ± 10.739	0.21	0.81	0.96
Tb.N (1/mm)	1.656 ± 0.105	1.779 ± 0.108	1.738 ± 0.082	1.762 ± 0.091	0.46	0.74	0.62
Tb.Th (mm)	0.060 ± 0.003	0.056 ± 0.003	0.052 ± 0.001	0.054 ± 0.003	0.56	0.07	0.27
Tb.Sp (mm)	0.611 ± 0.039	0.584 ± 0.037	0.588 ± 0.027	0.585 ± 0.32	0.67	0.74	0.72
Ct.Th (mm)	0.188 ± 0.007	0.177 ± 0.004	0.177 ± 0.004	0.174 ± 0.004	0.16	0.16	0.42
Ct.Ar (mm^2)	0.848 ± 0.042	0.777 ± 0.023	0.824 ± 0.019	0.780 ± 0.022	**0.04**	0.71	0.62
Ct.TMD (mg HA/cm^3)	1250.67 ± 5.63	1244.08 ± 4.89	1248.17 ± 4.93	1240.65 ± 4.39	0.16	0.55	0.93
Ma.Ar (mm^2)	1.115 ± 0.039	1.052 ± 0.033	1.210 ± 0.047	1.136 ± 0.032	0.08	**0.02**	0.89
Tt.Ar (mm^2)	1.965 ± 0.069	1.827 ± 0.044	2.032 ± 0.056	1.918 ± 0.043	**0.02**	0.14	0.81
Ct.Ar/Tt.Ar (%)	43.10 ± 1.18	42.56 ± 0.97	40.65 ± 0.92	40.71 ± 0.84	0.80	**0.03**	0.76
Ct. Porosity (%)	0.190 ± 0.014	0.209 ± 0.019	0.210 ± 0.011	0.236 ± 0.027	0.28	0.26	0.86
pMOI (mm^4)	0.438 ± 0.038	0.370 ± 0.018	0.440 ± 0.022	0.374 ± 0.027	**0.02**	0.91	0.98
I*max* (mm^4)	0.285 ± 0.029	0.237 ± 0.012	0.284 ± 0.017	0.246 ± 0.013	**0.02**	0.80	0.78
I*min* (mm^4)	0.153 ± 0.010	0.133 ± 0.006	0.157 ± 0.008	0.145 ± 0.007	0.051	0.33	0.65
Vertebral bone outcomes					***genotype***	***temperature***	***interaction***

BV/TV (%)	15.78 ± 1.20	13.14 ± 0.48	14.21 ± 1.23	12.02 ± 0.52	**0.01**	0.16	0.81
BS/BV (mm^2/mm^3)	38.163 ± 1.314	40.885 ± 1.093	41.505 ± 1.226	43.421 ± 1.734	0.10	**0.04**	0.77
BMD (mg HA/cm^3)	173.50 ± 11.92	148.38 ± 4.40	158.13 ± 11.54	137.50 ± 4.09	**0.02**	0.15	0.80
Conn.D (1/mm^3)	50.625 ± 9.160	47.838 ± 7.177	59.863 ± 6.764	48.050 ± 7.847	0.36	0.55	0.57
Tb.N (1/mm)	2.668 ± 0.070	2.425 ± 0.117	2.681 ± 0.110	2.436 ± 0.092	**0.02**	0.90	0.99
Tb.Th (mm)	0.061 ± 0.002	0.057 ± 0.002	0.056 ± 0.001	0.054 ± 0.002	0.15	0.06	0.64
Tb.Sp (mm)	0.382 ± 0.009	0.428 ± 0.024	0.384 ± 0.014	0.423 ± 0.016	**0.02**	0.90	0.83

Number of mice/group = 8 – 11 mice. BV/TV = bone volume fraction; Conn.D = connectivity densityTb.N = trabecular number; Tb.Th = trabecular thickness; Tb.Sp = trabecular separation; Ct.Th = average cortical thickness; Ct.Ar = cortical bone area; Ct.TMD = cortical tissue mineral density; M.Ar = marrow area; T.Ar = total cross-sectional area; Ct.Ar/T.Ar = cortical area fraction; Ct.Porosity = cortical porosity; pMOI = polar moment of inertia; Imax = maximum moment of inertia; Imin = minimum moment of inertia; BMD = bone mineral density; BS/BV =specific bone surface.

Discussion

In this study, we found evidence that *Trpm8* regulates adipose tissue metabolism in males. Our findings demonstrate that cold acclimation is both *Trpm8*- and sex-dependent. In this study, *Trpm8* deletion had a greater impact in male mice, who exhibited low core temperature at baseline and delayed cold acclimation. In female mice, *Trpm8* did not seem to be a necessary component for thermogenesis and core temperature regulation. Although we found evidence of poor thermoregulatory ability in males, cold exposure in the absence of *Trpm8* did not exacerbate bone loss, as we were expecting. In fact, we observed that both *Trpm8* deletion and cold exposure exerted independent effects on the skeleton. For instance, *Trpm8* deletion was mostly associated with reduced moment of inertia in both males and females, with female *Trpm8-KO* mice also exhibiting reduced cortical bone area. On the other hand, cold exposure affected femoral and vertebral trabecular bone volume in male, irrespective of the genotype (Figure 6).

Figure 6. Role of the *Trpm8* in thermoregulation, lipid and bone metabolism in male and female mice. *Trpm8* is a key player in the regulation of body temperature and lipid metabolism in male mice housed at room temperature (22°C). Concomitantly, *Trpm8* can also modulate bone homeostasis and its malfunction during development may interfere with cortical bone shape, leading to more fragile bone in male and female mice. In the absence of this cold-sensing channel, *Trpm8*-independent mechanisms (e.g. other *Trp* channels, shivering, and estrogen) can be activated and may play a more prominent role in the female adaptive response to cold exposure.

As previously mentioned, *Trpm8* allows the detection of environmental cooling [14,15,32] and it has also been implicated in BAT thermogenesis and thermoregulatory processes [1,20]. Early publications on *Trpm8* had reported no differences in core temperature associated with its global deletion in mice [32]. However, recently, Reimúndez et al. (2018) demonstrated that

Trpm8 seems to be important for body thermoregulation in male mice when housed in colder environments, which corroborates our findings [1]. Reimúndez et al. (2018) found that when males were housed at thermoneutrality, no changes in core temperature between genotypes (WT and Trpm8-KO) were observed, while at 21°C, the standard room temperature, those with *Trpm8* deletion started displaying reductions in their core temperature throughout daytime [1]. A significantly lower core temperature was only observed in male *Trpm8-KO* mice compared to WT littermates when housed at 17°C [1]. Interestingly, Reimúndez et al. (2017) also demonstrated that this difficulty in maintaining core temperature was associated with greater tail vasodilation and heat loss in male mice with global deletion of *Trpm8*, indicating that this cold-sensing channel has an important role in regulating both thermogenesis and heat dissipation [1].

Unfortunately, female core temperature status was not investigated in the studies mentioned above. However, Caudle et al. (2017) described sex differences in sensitivity to cool temperatures related to differences in the functioning of hyperpolarization-activated cyclic nucleotide-gated (HCN1) and voltage-gated potassium channels between male and female *Trpm8* expressing primary afferent neurons [33]. They found that male *Trpm8* trigeminal ganglia had larger menthol-induced inward currents than females that suggested a higher cool sensitivity in males. However, behavioral experiments demonstrated greater sensitivity to 18°C in female mice, which seemed to not be related to *Trpm8* action as cooling the neurons to 18°C did not visibly activate *Trpm8* in these trigeminal neurons [33].

Cooling sensitivity is the first step to activate the cold response neuronal mechanism that modulates lipolysis and energy expenditure [34]. Cold-induced metabolic changes are more pronounced in BAT compared to WAT depots [35]. Among the various types of WAT, subcutaneous WAT is more likely to acquire brown features compared to visceral or mesenteric WAT, which appear to be less responsive to cold challenge [35,36]. Liang et al. (2019) found

that a 4-hour acute cold treatment is enough to stimulate the expression of brown and beige adipocyte markers such as *Ucp1*, *Prdm16*, *Pgc1α*, *Cidea*, *Elovl3*, and *Pdk4* in subcutaneous WAT [37]. Moreover, WAT lipolysis induced by cold exposure seems to play a role in sustaining cold-induced BAT thermogenesis [35]. When exploring the early metabolomics response to 4 hour exposure at 4°C, Lu et al. (2017) observed that lipid metabolism was activated after 2 hours of cold exposure in both BAT and subcutaneous WAT [35]. Interestingly, they found that BAT lipolysis activity showed an oscillatory response to cold exposure as lipid metabolite levels returned to baseline at 4 hours and subsequently peaked again at 6 hours of cold exposure. Conversely, cold increased lipid metabolism in WAT after 2-4 hours of exposure, followed by a decrease towards baseline levels at 6 hours [35].

In our study, we observed that cold-induced weight loss occurred in both sexes, irrespective of the genotype. However, there were *Trpm8*- and sex-differences among the various adipose tissues' response to housing temperature. Male mice housed at 4°C exhibited BAT expansion with fewer lipid droplets and increased *Ucp1* expression in both genotypes, which is indicative of thermogenesis activity. A previous study demonstrated that reduced expression of thermogenic markers such as *Ucp1* was associated with loss of *Pparγ* expression, indicating that *Pparγ* has a role in the maintenance of BAT functionality [38]. However, in our study, *Pparγ2* expression, an adipose tissue specific factor, did not change in BAT with *Trpm8* deletion or cold exposure in male mice. Instead, we found that cold housing induced BAT expression of other fatty acid metabolism markers (*Acadl, Prdm16,* and *Pgc1α*) as well as a robust expression of other thermogenic markers such as *Cidea* and *Dio2* in BAT of male *Trpm8-KO* mice. Lipolysis is considered an essential step to induce thermogenesis in BAT during cold exposure. Conversely, there is also evidence that lipolysis is not energetically critical for heat production in BAT. Others have observed that in the absence of BAT lipolysis during cold acclimation, thermoregulation is supported by iWAT lipolysis under fasting conditions or by

diet nutrients [34]. However, in our study, long-term cold challenge had no effect on iWAT weight. Instead, we found cold exposure had a greater impact on gWAT weight in females and increased expression of *Ucp1* in male *Trpm8-KO* mice. There were no other changes in the expression of fatty acid metabolism and other thermogenic markers in male *Trpm8-KO* gWAT.

Nevertheless, it should be considered that both the cold acclimation period, as well as the duration of cold exposure, can have diverse effects on thermogenesis and the WAT beiging process [39,40]. Previously, Ukropec et al. (2006) found that mice lacking *Ucp1* can better tolerate cold at 4°C when progressively acclimated to cold [39]. Moreover, while acute cold treatment has been reported to stimulate subcutaneous WAT beiging [37], a chronic cold treatment seems to reduce mitochondrial numbers and *Ucp1* and *Prdm16* expression in subcutaneous WAT [40]. This could explain the different response to cold exposure that we observed between types of WAT which might be related to the duration of the challenge and the progressive acclimation from 22°C to 4°C housing.

In females, we found that *Trpm8* deletion led to an increase in *Ucp1* expression in BAT during cold exposure. Perhaps the most striking finding was that this response to cold exposure was independent of *Trpm8* deletion. In response to cold, we found a significant reduction in gWAT mass in female mice from both genotypes, corresponding to increased expression of fatty acid metabolism (*Acadl, Pgc1α, Pdk4*), and thermogenic (*Ucp1, Cidea, Dio2*) markers. It should be considered that estrogen can play a role in sex-differences in thermogenesis and WAT beiging found in the present study. Several studies observed that the beiging process does take place in gWAT in females [36,41]. Increased expression of beiging markers such as *Ucp1*, *Pgc1α*, *Elovl3*, *Cidea* was observed in gWAT after either 10 days of cold exposure [36] or β3-adrenergic receptor agonist treatment [41] in female mice. Kim et al. (2016) demonstrated that gWAT in females is more susceptible to the beiging process than in males, due to more

extensive sympathetic innervation inducing brown adipogenesis [41]. Also, the authors showed that sympathetic innervation of gWAT is sex-hormone dependent, as reduced tyrosine hydroxylase protein levels and lack of beiging of gWAT was found after chemical ovarian ablation [41]. Indeed, lipolysis can be directly modulated by estrogen through estrogen receptor alpha (ERα) signaling in BAT and WAT adipocytes [42]. Estrogen also has been described to play a critical role in cold sensitivity and hyperalgesia [43,44], which are also functions thought to be regulated by *Trpm8* [33,45]. However, interestingly, a previous preclinical study observed that *Trpm8* expression was upregulated in the skin of ovariectomized rats compared to sham control rats [46] and β-estradiol treatment might reduce *Trpm8* overexpression in the skin of ovariectomized rats [47]. These findings support our data that suggest that regulation of energy metabolism in female mice is independent of *Trpm8* cold-sensing function and estrogen might be a more relevant factor to normal thermoregulation.

Surprisingly, in opposition to our hypothesis, there was no interaction effect between the mouse genotype and the housing temperature on bone outcomes other than BMAT in females. We found that cold exposure led to reduced trabecular bone volume in males and cortical area fraction in females which is consistent with previous studies showing that cold exposure can negatively impact the skeleton [2,13]. It has previously been shown that cold exposure is associated with reduced BMAT [48], but our findings indicate that in females this may be dependent upon *Trpm8*. On the other hand, a novel finding was that the absence of *Trpm8* was associated with impaired bone strength-related measures in both male and female mice. However, cold exposure did not exacerbated this negative effect on cortical bone of mice with *Trpm8* deletion.

Recently, Iwaniec et al. (2016) highlighted that the current standard room temperature housing (22°C) can already be considered a cold environment to mice and that it was associated with bone loss in growing females compared to thermoneutral housing [2]. A *Trpm8*

functional cold circuit is established after birth around postnatal day 14 [49]. We and others [1,18,20] have found that *Trpm8* is a regulator of energy metabolism and thermogenesis activity and our findings show that its deletion can cause an increase in the expression of thermogenic markers, gWAT fat pad reduction and weight loss. This suggests that the absence of *Trpm8* during the developmental phase might be associated with defective cold circuits which partially fail to sustain optimal body temperature, as previously described [1]. Thus, it is plausible that the lack of *Trpm8* during growth causes a shift towards energy utilization for heat generation, decreasing ATP availability for bone cells, which is detrimental to bone integrity, leading to a more fragile mature bone. Recent evidence confirms that bone cells require a substantial amount of ATP to maintain an optimal bone turnover. Rendina-Ruedy et al. (2017) found increased expression of adipose differentiation-related protein (ADRP, *Plin2*) in *in vitro* assays and in femur cortex and bone marrow samples *in vivo*, demonstrating that fatty acids from the bone marrow microenvironment are a main source of energy for osteoblasts at early stages of differentiation [50]. In our study, however, we found no differences in adipocyte content within the bone marrow in males. We actually observed that *Trpm8* deletion in females was not only associated with reduced gWAT, but also with a decreased BMAT content. Recently, Wee et al., (2019) elegantly demonstrated that iWAT and BMAT shared sympathetic innervation as well as energy utilization and lipolysis [51]. They revealed that leptin-responsive regions such as paraventricular hypothalamus, arcuate nucleus, dorsomedial hypothalamus, ventromedial hypothalamus, and area postrema were labelled after viral tracing from iWAT, bone marrow, and BMAT [51]. However, it is important to consider that most of the experiments were performed in male mice, and sex-differences related to common pathways between iWAT and BMAT in females, and the shared pathways between gWAT and BMAT still needs to be further explored. This investigation would be extremely relevant as gWAT seems to be a source of energy under cold conditions for female mice. In summary, our findings support that *Trpm8* is important for body temperature maintenance in male mice and its absence triggers a

compensatory response to counteract reduction in core temperature. Moreover, *Trpm8* does not appear to regulate bone homeostasis in colder environments, where it is presumed that the SNS contributes to bone loss. However, deletion of *Trpm8* was associated with cortical bone shape indicative of more fragile bone, irrespective of sex. Therefore, bone loss found after cold exposure was independent of *Trpm8* channel.

One limitation of our study is that we have not assessed the potential contributions of the compensatory *Trpm8*-independent mechanisms (e.g. other Trp channels, shivering, and estrogen) to our findings. Cold exposure also activates other mechanisms, which could have compensated for *Trpm8* absence. First, in addition to *Trpm8*, there is another cold-activated *Trp* channel known as transient receptor potential ankyrin 1 (*Trpa1*) which is considered to be a noxious cold receptor [52]. Interestingly, *Trpm8* and *Trpa1* appear to function in both complementary and synergistic fashion to detect environmental innocuous and noxious cold [52]. Winter et al. (2017) found that the lack of *Trpm8* and *Trpa1* led to a striking reduction in cold avoidance behavior in mice [52]. However, an acute cold avoidance response was still observed in *Trpm8-KO* mice with functional *Trpa1* when exposed to a temperature range between 28°C and 15°C [52]. This suggests that *Trpa1* can compensate for *Trpm8* absence, even though *Trpa1* response to cold-sensing seems to be smaller compared to *Trpm8* [52].

Secondly, when cold-defense mechanisms, such as thermogenesis and vascular tone, fail to sustain an optimal body temperature, a shivering response is triggered to increase heat generation [53] that we have not investigated in the present study. However, it is worth mentioning that previous studies found that *Trpm8* is not required to induce shivering and tachycardia during cold challenge [53]. Instead, shivering is found to be regulated by *Trpv1* [53], which once more indicates *Trpm8* as a major regulator of non-shivering thermogenesis. Additionally, this reinforces the complexity of the role of *Trp* channels in thermo-sensation and thermoregulation as well as the intricate inter-connection of various *Trp* channels.

We also have not further investigated the effects of *Trpm8* deletion on metabolic outcomes (e.g. energy expenditure, respiratory quotient). However, the current data provide new insight into our understanding of the role of *Trpm8* in the regulation of thermogenesis and skeletal homeostasis and demonstrate important and unexpected sex-differences in these processes. Finally, though we saw reductions in bone strength indicators (moments of inertia) with *Trpm8* deletion, we did not actually perform mechanical testing to determine if *Trpm8* deletion leads to reduced bone strength. Nonetheless, this work suggests that although bone and adipose tissue metabolism are regulated by *Trpm8*, mechanisms and consequences of this regulation are tissue- and sex-dependent and require further investigation.

Acknowledgments

The authors thank Phuong Le and Casey Doucette for the assistance during the cold housing experiment. This work was supported by the National Institute of Arthritis And Musculoskeletal And Skin Diseases (NIAMS) and the National Institute of General Medical Sciences (NIGMS) of the National Institutes of Health (NIH) under award numbers K01AR067858 and P20GM121301 to KJM. This work utilized services of the Maine Medical Center Research Institute (MMCRI) Molecular Phenotyping Core, which is supported by NIH/NIGMS P30GM106391, the Physiology Core, which is supported by NIH/NIGMS P30GM106391 and P20GM121301, the Histopathology and Histomorphometry Core, which is supported by NIH/NIGMS P30GM106391, P20GM121301, and P30103392, and the Mouse Transgenic and In Vivo Imaging Core which is supported by NIH/NIGMS P30GM103392. All cores also received support from the Norther New England Clinical and Translational Research Network NIH/NIGMS U54GM115516. The content is solely the responsibility of the authors and does not necessarily represent the official views of the National Institutes of Health.

Authors Contributions

ALC was responsible for data acquisition, data analysis, interpretation, drafting and critical review of the manuscript. AT was responsible for data acquisition, data analysis, interpretation, drafting and critical review of the manuscript. DJB was responsible for data acquisition, data analysis, interpretation, drafting and critical review of the manuscript. SC was responsible for data acquisition, data analysis, interpretation, drafting and critical review of the manuscript. MRR was responsible for data interpretation and critical review of the manuscript. MLB was responsible for data interpretation and critical review of the manuscript. KJM was responsible for experimental design, data acquisition, data analysis, interpretation, drafting, and critical review of the manuscript. All authors had final approval of the manuscript.

Declaration of interests

The authors have declared that no conflict of interest exists.

References

1. Reimúndez A, Fernández-Peña C, García G, Fernández R, Ordás P, Gallego R, et al. Deletion of the cold thermoreceptor TRPM8 increases heat loss and food intake leading to reduced body temperature and obesity in mice. J Neurosci. 2018;38: 3643–3656. doi:10.1523/JNEUROSCI.3002-17.2018
2. Iwaniec UT, Philbrick KA, Wong CP, Gordon JL, Kahler-Quesada AM, Olson DA, et al. Room temperature housing results in premature cancellous bone loss in growing female mice: implications for the mouse as a preclinical model for age-related bone loss. Osteoporos Int. 2016;27: 3091–3101. doi:10.1007/s00198-016-3634-3
3. Fedorenko A, Lishko P V., Kirichok Y. Mechanism of fatty-acid-dependent UCP1 uncoupling in brown fat mitochondria. Cell. 2012;151: 400–413. doi:10.1016/j.cell.2012.09.010

4. Tan CL, Knight ZA. Regulation of Body Temperature by the Nervous System. Neuron. 2018;98: 31–48. doi:10.1016/j.neuron.2018.02.022

5. Contreras GA, Lee YH, Mottillo EP, Granneman JG. Inducible brown adipocytes in subcutaneous inguinal white fat: The role of continuous sympathetic stimulation. Am J Physiol - Endocrinol Metab. 2014;307: E793–E799. doi:10.1152/ajpendo.00033.2014

6. Bahler L, Verberne HJ, Admiraal WM, Stok WJ, Soeters MR, Hoekstra JB, et al. Differences in sympathetic nervous stimulation of brown adipose tissue between the young and old, and the lean and obese. J Nucl Med. 2016;57: 372–377. doi:10.2967/jnumed.115.165829

7. Liu CK. the Impact of Sarcopenia on a Physical Activity Intervention : the Lifestyle Interventions and. J Nutr Heal Aging. 2014;18: 59–64. doi:10.1007/s12603-013-0369-0.THE

8. Zoico E, Rubele S, De Caro A, Nori N, Mazzali G, Fantin F, et al. Brown and beige adipose tissue and aging. Front Endocrinol (Lausanne). 2019;10: 1–10. doi:10.3389/fendo.2019.00368

9. Wang W, Ishibashi J, Trefely S, Shao M, Cowan AJ, Sakers A, et al. A PRDM16-Driven Metabolic Signal from Adipocytes Regulates Precursor Cell Fate. Cell Metab. 2019;30: 174-189.e5. doi:10.1016/j.cmet.2019.05.005

10. Johnell O, Kanis JA. An estimate of the worldwide prevalence and disability associated with osteoporotic fractures. Osteoporos Int. 2006;17: 1726–1733. doi:10.1007/s00198-006-0172-4

11. Odén A, McCloskey E V., Kanis JA, Harvey NC, Johansson H. Burden of high fracture probability worldwide: secular increases 2010–2040. Osteoporos Int. 2015;26: 2243–2248. doi:10.1007/s00198-015-3154-6

12. Elefteriou F. Neuronal signaling and the regulation of bone remodeling. Cell Mol Life Sci. 2005;62: 2339–2349. doi:10.1007/s00018-005-5175-3

13. Motyl KJ, Bishop KA, Demambro VE, Bornstein SA, Le P, Kawai M, et al. Altered thermogenesis and impaired bone remodeling in Misty mice. J Bone Miner Res. 2013;28: 1885–1897. doi:10.1002/jbmr.1943

14. Dhaka A, Murray AN, Mathur J, Earley TJ, Petrus MJ, Patapoutian A. TRPM8 Is Required for Cold Sensation in Mice. Neuron. 2007;54: 371–378. doi:10.1016/j.neuron.2007.02.024

15. McKemy DD, Neuhausser WM, Julius D. Identification of a cold receptor reveals a general role for TRP channels in thermosensation. Nature. 2002;416: 52–58. doi:10.1038/nature719

16. Zhu Z, Ma S, Yu H, Zhao Z, Luo Z, Chen J, et al. Activation of the cold-sensing TRPM8 channel triggers UCP1-dependent thermogenesis and prevents obesity. J Mol Cell Biol. 2012;4: 88–96. doi:10.1093/jmcb/mjs001

17. McCoy DD, Zhou L, Nguyen AK, Watts AG, Donovan CM, McKemy DD. Enhanced insulin clearance in mice lacking TRPM8 channels. Am J Physiol - Endocrinol Metab. 2013;305: 78–88. doi:10.1152/ajpendo.00542.2012

18. Rossato M, Granzotto M, Macchi V, Porzionato A, Petrelli L, Calcagno A, et al. Human white adipocytes express the cold receptor TRPM8 which activation induces UCP1 expression, mitochondrial activation and heat production. Mol Cell Endocrinol. 2014;383: 137–146. doi:10.1016/j.mce.2013.12.005

19. Moraes MN, de Assis LVM, Henriques F dos S, Batista ML, Güler AD, Castrucci AM de L. Cold-sensing TRPM8 channel participates in circadian control of the brown adipose tissue. Biochim Biophys Acta - Mol Cell Res. 2017;1864: 2415–2427. doi:10.1016/j.bbamcr.2017.09.011

20. Jiang C, Zhai M, Yan D, Li D, Li C, Zhang Y, et al. Dietary menthol-induced TRPM8 activation enhances WAT 1C “browning 1D” and ameliorates diet-induced obesity. Oncotarget. 2017;8: 75114–75126. doi:10.18632/oncotarget.20540

21. Abed E, Labelle D, Martineau C, Loghin A, Moreau R. Expression of transient receptor potential (TRP) channels in human and murine osteoblast-like cells. Mol Membr Biol. 2009;26: 146–158. doi:10.1080/09687680802612721

22. Takahashi N, Matsuda Y, Sato K, De Jong PR, Bertin S, Tabeta K, et al. Neuronal TRPV1 activation regulates alveolar bone resorption by suppressing osteoclastogenesis via CGRP. Sci Rep. 2016;6: 1–11. doi:10.1038/srep29294

23. Nilius B, Voets T, Peters J. TRP channels in disease. Sci STKE. 2005;2005: 1–10.

24. Motyl KJ, DeMambro VE, Barlow D, Olshan D, Nagano K, Baron R, et al. Propranolol attenuates risperidone-induced trabecular bone loss in female mice. Endocrinology. 2015;156: 2374–2383. doi:10.1210/en.2015-1099

25. Eliceiri K, Schneider CA, Rasband WS, Eliceiri KW. NIH Image to ImageJ : 25 years of image analysis HISTORICAL commentary NIH Image to ImageJ : 25 years of image analysis. Nat Methods. 2012;9: 671–675. doi:10.1038/nmeth.2089

26. T. Ferreira WR. ImageJ User Guide IJ 1.46r. IJ 146r. 2012; 185. doi:10.1038/nmeth.2019

27. Bouxsein ML, Boyd SK, Christiansen BA, Guldberg RE, Jepsen KJ, Müller R. Guidelines for assessment of bone microstructure in rodents using micro-computed tomography. J Bone Miner Res. 2010;25: 1468–1486. doi:10.1002/jbmr.141

28. Vengellur A, LaPres JJ. The role of hypoxia inducible factor 1α in cobalt chloride induced cell death in mouse embryonic fibroblasts. Toxicol Sci. 2004;82: 638–646. doi:10.1093/toxsci/kfh278

29. Seale et al. PRDM16 Controls a Brown Fat/Skeletal Muscle Switch. Bone. 2008;23: 1–7. doi:10.1038/nature07182

30. Sanchez-Gurmaches ; Guertin D. Adipocytes arise from multiple lineages that are heterogeneously and dynamically distributed Access. Nat Commun. 2014;5: 4099. doi:10.1038/ncomms5099

31. Cooper MP, Uldry M, Kajimura S, Arany Z, Spiegelman BM. Modulation of PGC-1

coactivator pathways in brown fat differentiation through LRP130. J Biol Chem. 2008;283: 31960–31967. doi:10.1074/jbc.M805431200

32. Bautista DM, Siemens J, Glazer JM, Tsuruda PR, Basbaum AI, Stucky CL, et al. The menthol receptor TRPM8 is the principal detector of environmental cold. Nature. 2007;448: 204–208. doi:10.1038/nature05910

33. Caudle RM, Caudle SL, Jenkins AC, Ahn AH, Neubert JK. Sex differences in mouse Transient Receptor Potential Cation Channel, Subfamily M, Member 8 expressing trigeminal ganglion neurons. PLoS One. 2017;12: 1–20. doi:10.1371/journal.pone.0176753

34. Shin H, Ma Y, Chanturiya T, Cao Q, Wang Y, Kadegowda AKG, et al. Lipolysis in Brown Adipocytes Is Not Essential for Cold-Induced Thermogenesis in Mice. Cell Metab. 2017;26: 764-777.e5. doi:10.1016/j.cmet.2017.09.002

35. Lu X, Solmonson A, Lodi A, Nowinski SM, Sentandreu E, Riley CL, et al. The early metabolomic response of adipose tissue during acute cold exposure in mice. Sci Rep. 2017;7: 1–11. doi:10.1038/s41598-017-03108-x

36. Rosell M, Kaforou M, Frontini A, Okolo A, Chan YW, Nikolopoulou E, et al. Brown and white adipose tissues: Intrinsic differences in gene expression and response to cold exposure in mice. Am J Physiol - Endocrinol Metab. 2014;306. doi:10.1152/ajpendo.00473.2013

37. Liang X, Pan J, Cao C, Zhang L, Zhao Y, Fan Y, et al. Transcriptional response of subcutaneous white adipose tissue to acute cold exposure in mice. Int J Mol Sci. 2019;20. doi:10.3390/ijms20163968

38. Lasar D, Rosenwald M, Kiehlmann E, Balaz M, Tall B, Opitz L, et al. Peroxisome Proliferator Activated Receptor Gamma Controls Mature Brown Adipocyte Inducibility through Glycerol Kinase. Cell Rep. 2018;22: 760–773. doi:10.1016/j.celrep.2017.12.067

39. Ukropec J, Anunciado RP, Ravussin Y, Hulver MW, Kozak LP. UCP1-independent

thermogenesis in white adipose tissue of cold-acclimated Ucp1-/- mice. J Biol Chem. 2006;281: 31894–31908. doi:10.1074/jbc.M606114200

40. Gao Y, Qimuge NR, Qin J, Cai R, Li X, Chu GY, et al. Acute and chronic cold exposure differentially affects the browning of porcine white adipose tissue. Animal. 2018;12: 1435–1441. doi:10.1017/S1751731117002981

41. Kim SN, Jung YS, Kwon HJ, Seong JK, Granneman JG, Lee YH. Sex differences in sympathetic innervation and browning of white adipose tissue of mice. Biol Sex Differ. 2016;7: 1–13. doi:10.1186/s13293-016-0121-7

42. Clookey SL, Welly RJ, Shay D, Woodford ML, Fritsche KL, Rector RS, et al. Beta 3 adrenergic receptor activation rescues metabolic dysfunction in female estrogen receptor alpha-null mice. Front Physiol. 2019;10: 1–15. doi:10.3389/fphys.2019.00009

43. Cankar K, Music M, Finderle Z. Cutaneous microvascular response during local cold exposure - the effect of female sex hormones and cold perception. Microvasc Res. 2016;108: 34–40. doi:10.1016/j.mvr.2016.07.006

44. Smeester BA, O'Brien EE, Michlitsch KS, Lee JH, Beitz AJ. The relationship of bone-tumor-induced spinal cord astrocyte activation and aromatase expression to mechanical hyperalgesia and cold hypersensitivity in intact female and ovariectomized mice. Neuroscience. 2016;324: 344–354. doi:10.1016/j.neuroscience.2016.03.030

45. Weyer AD, Lehto SG. Development of TRPM8 antagonists to treat chronic pain and migraine. Pharmaceuticals. 2017;10: 1–9. doi:10.3390/ph10020037

46. Noguchi W, Ishizuka O, Imamura T, Kurizaki Y, Yamagishi T, Yokoyama H, et al. The relationship between α1-adrenergic receptors and TRPM8 channels in detrusor overactivity induced by cold stress in ovariectomized rats. J Urol. 2013;189: 1975–1981. doi:10.1016/j.juro.2012.10.014

47. Kubo T, Tsuji S, Amano T, Yoshino F, Niwa Y, Kasahara K, et al. Effects of β-estradiol on cold-sensitive receptor channel TRPM8 in ovariectomized rats. Exp Anim. 2017;66: 337–

343. doi:10.1538/expanim.17-0028

48. Scheller EL, Doucette CR, Learman BS, Cawthorn WP, Khandaker S, Schell B, et al. Region-specific variation in the properties of skeletal adipocytes reveals regulated and constitutive marrow adipose tissues. Nat Commun. 2015;6: 1–13. doi:10.1038/ncomms8808

49. Takashima Y, Ma L, McKemy DD. The development of peripheral cold neural circuits based on TRPM8 expression. Neuroscience. 2010;169: 828–842. doi:10.1016/j.neuroscience.2010.05.039

50. Rendina-Ruedy E, Guntur AR, Rosen CJ. Intracellular lipid droplets support osteoblast function. Adipocyte. 2017;6: 250–258. doi:10.1080/21623945.2017.1356505

51. Wee NKY, Lorenz MR, Bekirov Y, Jacquin MF, Scheller EL. Shared autonomic pathways connect bone marrow and peripheral adipose tissues across the central neuraxis. Front Endocrinol (Lausanne). 2019;10: 1–16. doi:10.3389/fendo.2019.00668

52. Winter Z, Gruschwitz P, Eger S, Touska F, Zimmermann K. Cold temperature encoding by cutaneous TRPA1 and TRPM8-carrying fibers in the mouse. Front Mol Neurosci. 2017;10. doi:10.3389/fnmol.2017.00209

53. Feketa V V., Balasubramanian A, Flores CM, Player MR, Marrelli SP. Shivering and tachycardic responses to external cooling in mice are substantially suppressed by TRPV1 activation but not by TRPM8 inhibition. Am J Physiol - Regul Integr Comp Physiol. 2013;305: 1040–1050. doi:10.1152/ajpregu.00296.2013

Supplemental References

Cooper, M.P., Uldry, M., Kajimura, S., Arany, Z., Spiegelman, B.M., 2008. Modulation of PGC-1 coactivator pathways in brown fat differentiation through LRP130. J. Biol. Chem. 283, 31960–31967. https://doi.org/10.1074/jbc.M805431200

Sanchez-Gurmaches ; Guertin, D., 2014. Adipocytes arise from multiple lineages that are heterogeneously and dynamically distributed Access. Nat Commun. 5, 4099. https://doi.org/10.1038/ncomms5099

Seale et al., 2008. PRDM16 Controls a Brown Fat/Skeletal Muscle Switch. Bone 23, 1–7. https://doi.org/10.1038/nature07182

A

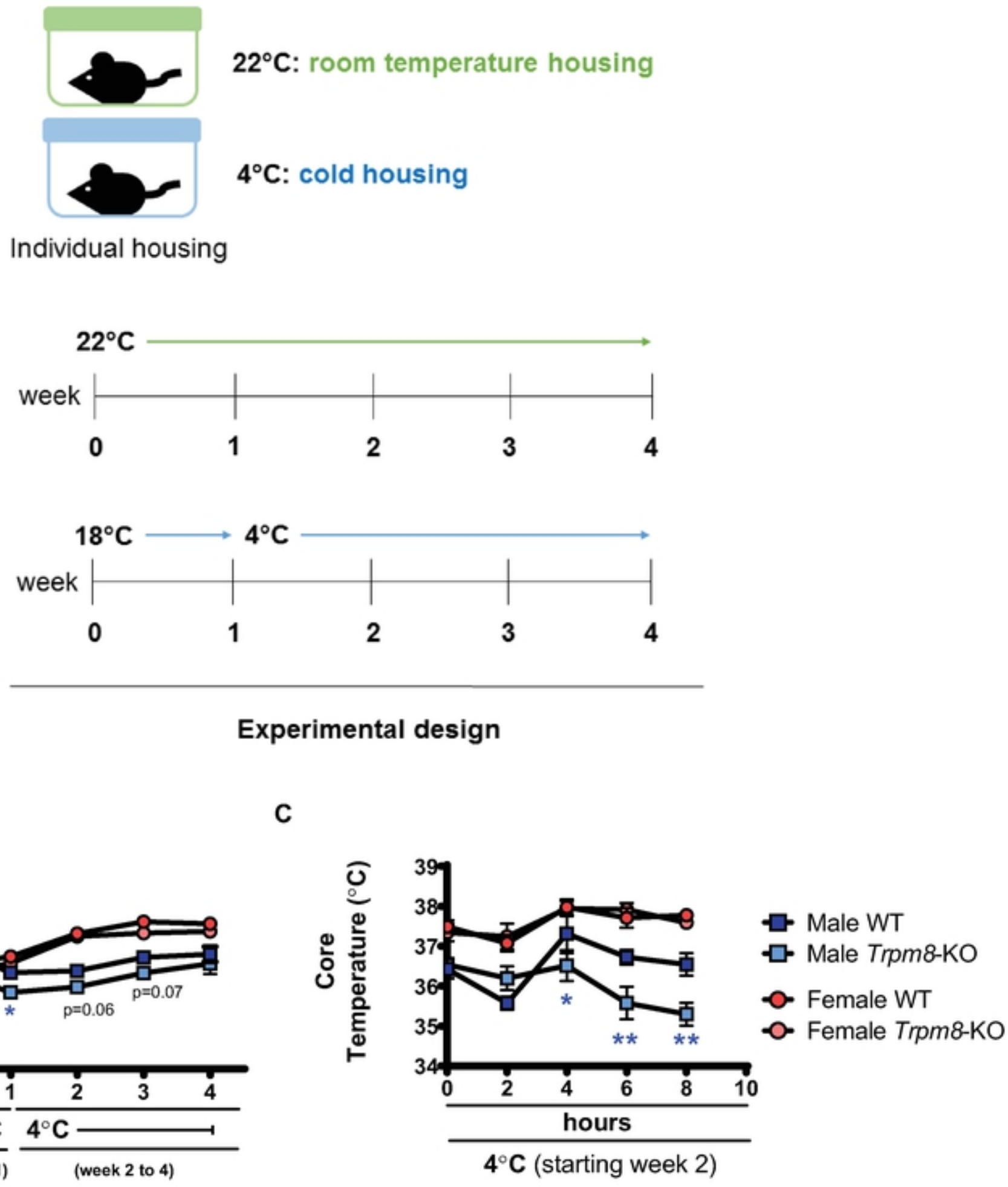
22°C: room temperature housing
4°C: cold housing
Individual housing
22°C
week
0
1
2
3
4
18°C
4°C
week
0
1
2
3
4
Experimental design
B
Core Temperature (°C)
40
39
38
37
36
35
34
**
*
p=0.06
p=0.07
Week →
0
1
2
3
4
18°C
4°C
(week 1)
(week 2 to 4)
C
Core Temperature (°C)
39
38
37
36
35
34
*
**
**
0
2
4
6
8
10
hours
4°C (starting week 2)
Male WT
Male Trpm8-KO
Female WT
Female Trpm8-KO

Figure 1

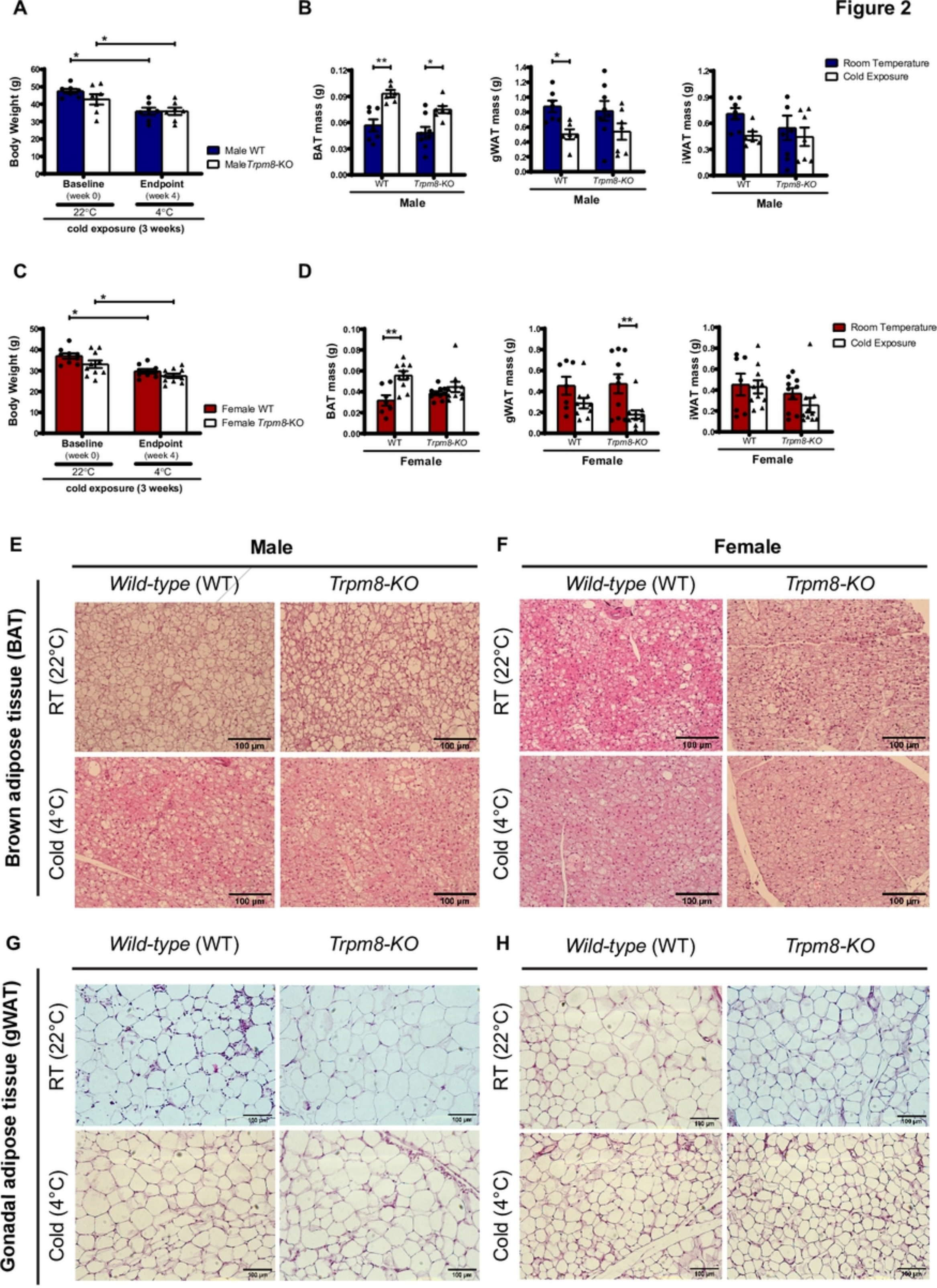
Figure 2
A
Body Weight (g)
Male WT
Male Trpm8-KO
Baseline (week 0)
Endpoint (week 4)
22°C
4°C
cold exposure (3 weeks)
B
BAT mass (g)
gWAT mass (g)
iWAT mass (g)
WT
Trpm8-KO
Male
Room Temperature
Cold Exposure
C
Female WT
Female Trpm8-KO
D
Female
E
Male
Wild-type (WT)
Trpm8-KO
Brown adipose tissue (BAT)
RT (22°C)
Cold (4°C)
100 µm
F
Female
G
Gonadal adipose tissue (gWAT)
H

Figure 2

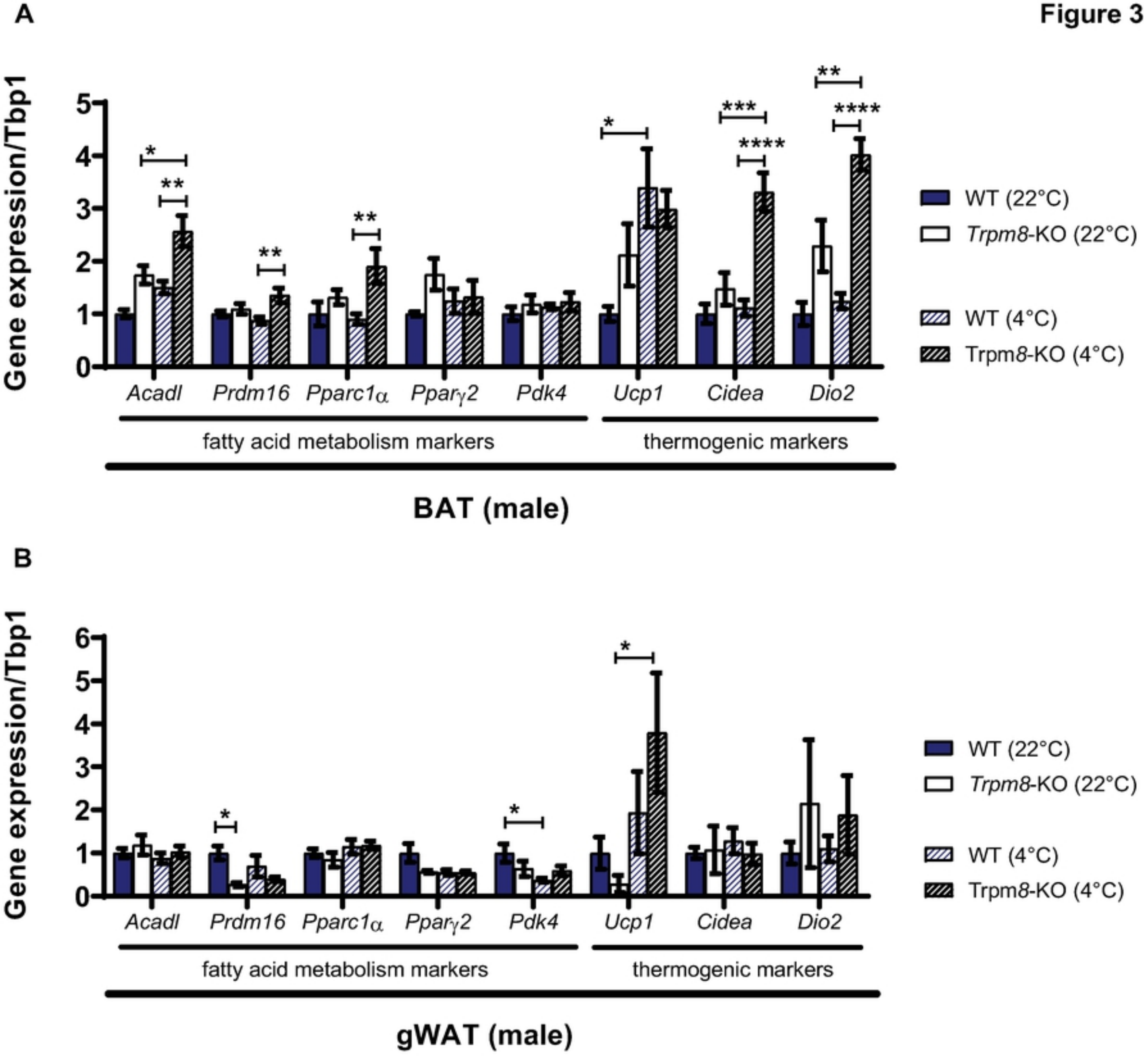
A
Figure 3
Gene expression/Tbp1
5
4
3
2
1
0
*
**
**
**
*
***
****
**
****
Acadl
Prdm16
Pparc1α
Pparγ2
Pdk4
Ucp1
Cidea
Dio2
fatty acid metabolism markers
thermogenic markers
BAT (male)
WT (22°C)
Trpm8-KO (22°C)
WT (4°C)
Trpm8-KO (4°C)
B
Gene expression/Tbp1
6
5
4
3
2
1
0
*
*
*
Acadl
Prdm16
Pparc1α
Pparγ2
Pdk4
Ucp1
Cidea
Dio2
fatty acid metabolism markers
thermogenic markers
gWAT (male)
WT (22°C)
Trpm8-KO (22°C)
WT (4°C)
Trpm8-KO (4°C)

Figure 3

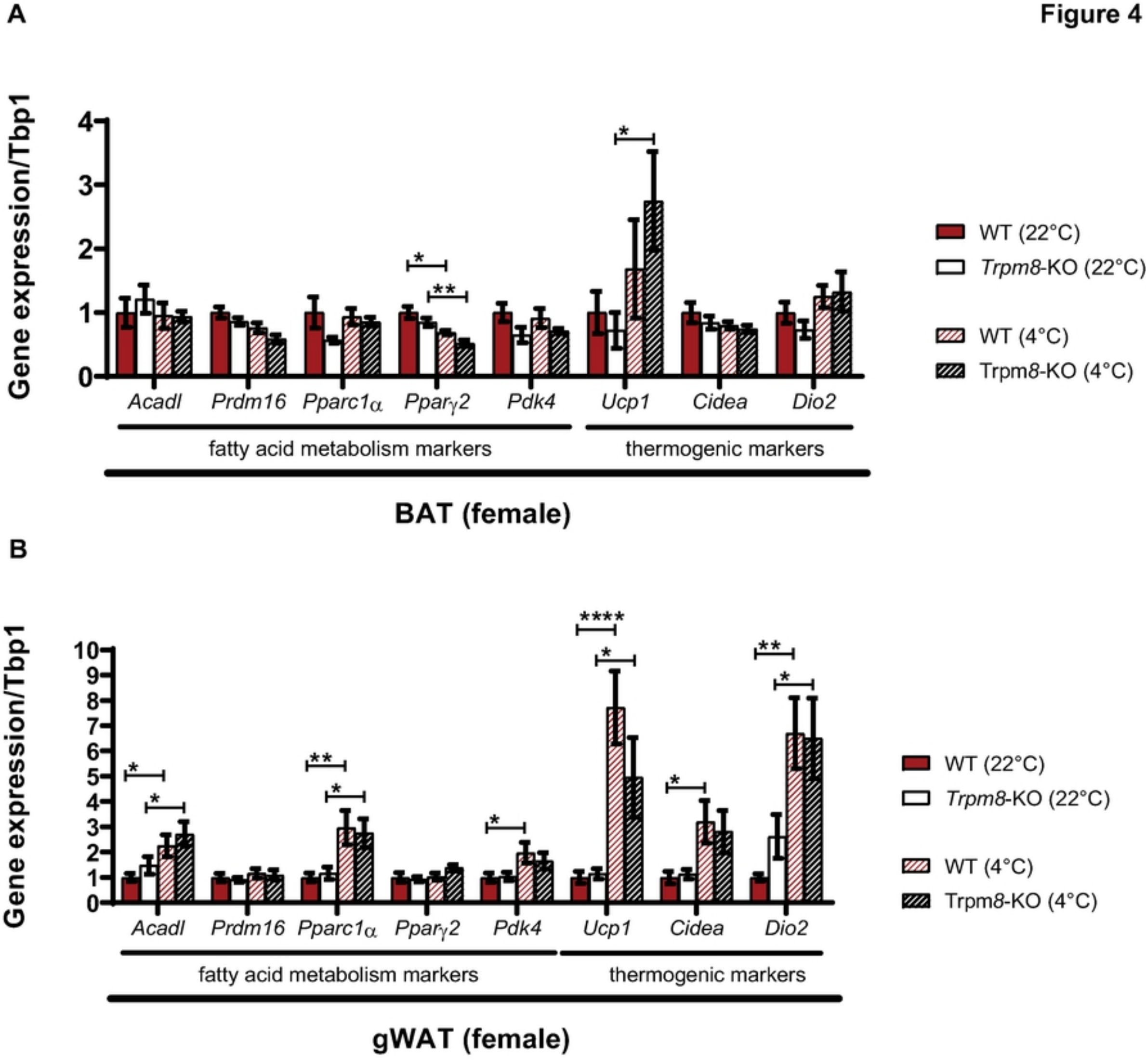
A
Figure 4
Gene expression/Tbp1
4
3
2
1
0
*
**
*
Acadl
Prdm16
Pparc1α
Pparγ2
Pdk4
Ucp1
Cidea
Dio2
fatty acid metabolism markers
thermogenic markers
BAT (female)
WT (22°C)
Trpm8-KO (22°C)
WT (4°C)
Trpm8-KO (4°C)
B
Gene expression/Tbp1
10
9
8
7
6
5
4
3
2
1
0
****
*
**
*
*
**
*
*
*
Acadl
Prdm16
Pparc1α
Pparγ2
Pdk4
Ucp1
Cidea
Dio2
fatty acid metabolism markers
thermogenic markers
gWAT (female)
WT (22°C)
Trpm8-KO (22°C)
WT (4°C)
Trpm8-KO (4°C)

Figure 4

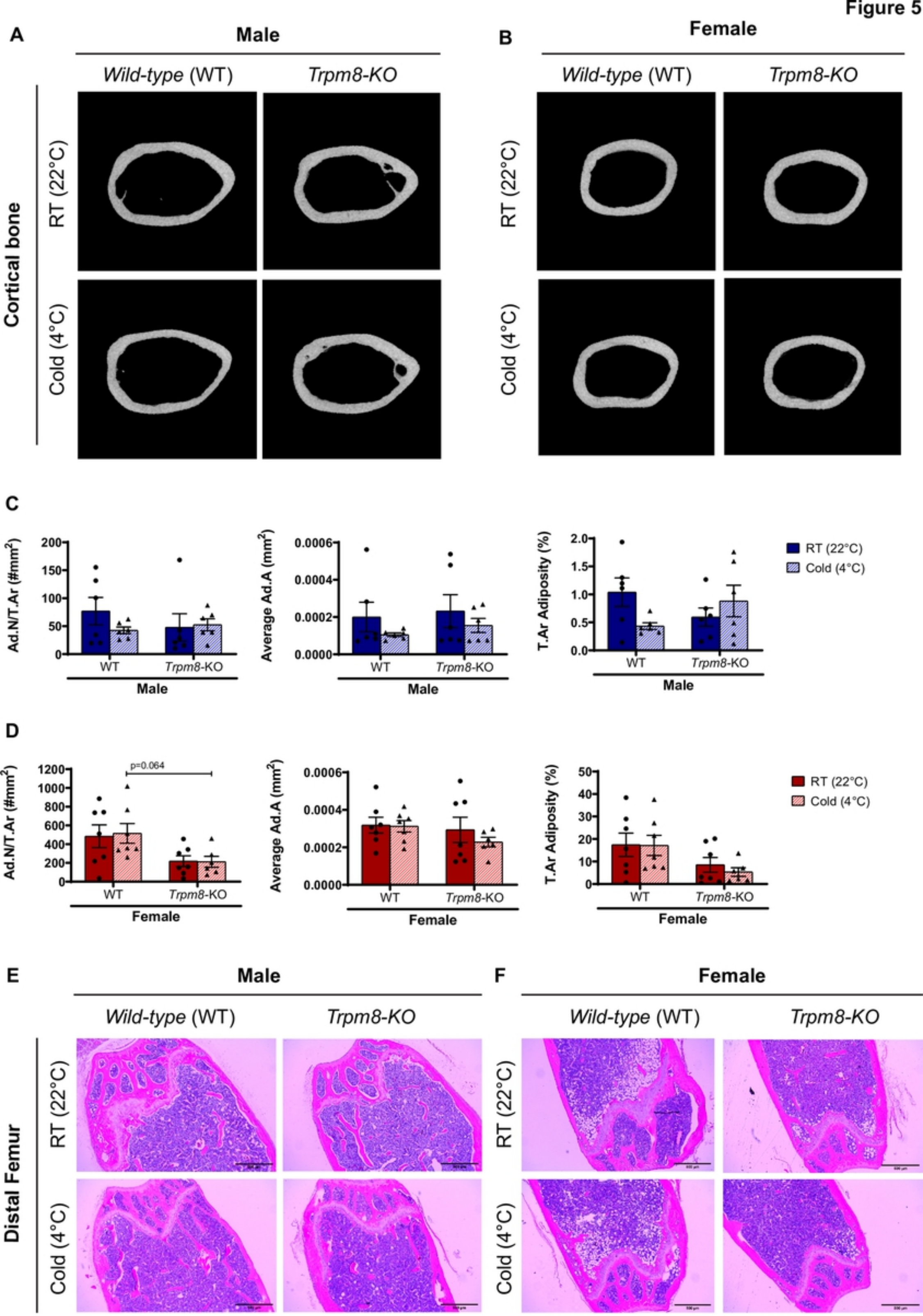
A
Male
Wild-type (WT)
Trpm8-KO
Cortical bone
RT (22°C)
Cold (4°C)
B
Female
Wild-type (WT)
Trpm8-KO
RT (22°C)
Cold (4°C)
C
Ad.N/T.Ar (#mm²)
Average Ad.A (mm²)
T.Ar Adiposity (%)
RT (22°C)
Cold (4°C)
WT
Trpm8-KO
Male
D
p=0.064
Ad.N/T.Ar (#mm²)
Average Ad.A (mm²)
T.Ar Adiposity (%)
RT (22°C)
Cold (4°C)
WT
Trpm8-KO
Female
E
Male
Wild-type (WT)
Trpm8-KO
Distal Femur
RT (22°C)
Cold (4°C)
F
Female
Wild-type (WT)
Trpm8-KO
RT (22°C)
Cold (4°C)

Figure 5

Figure 6

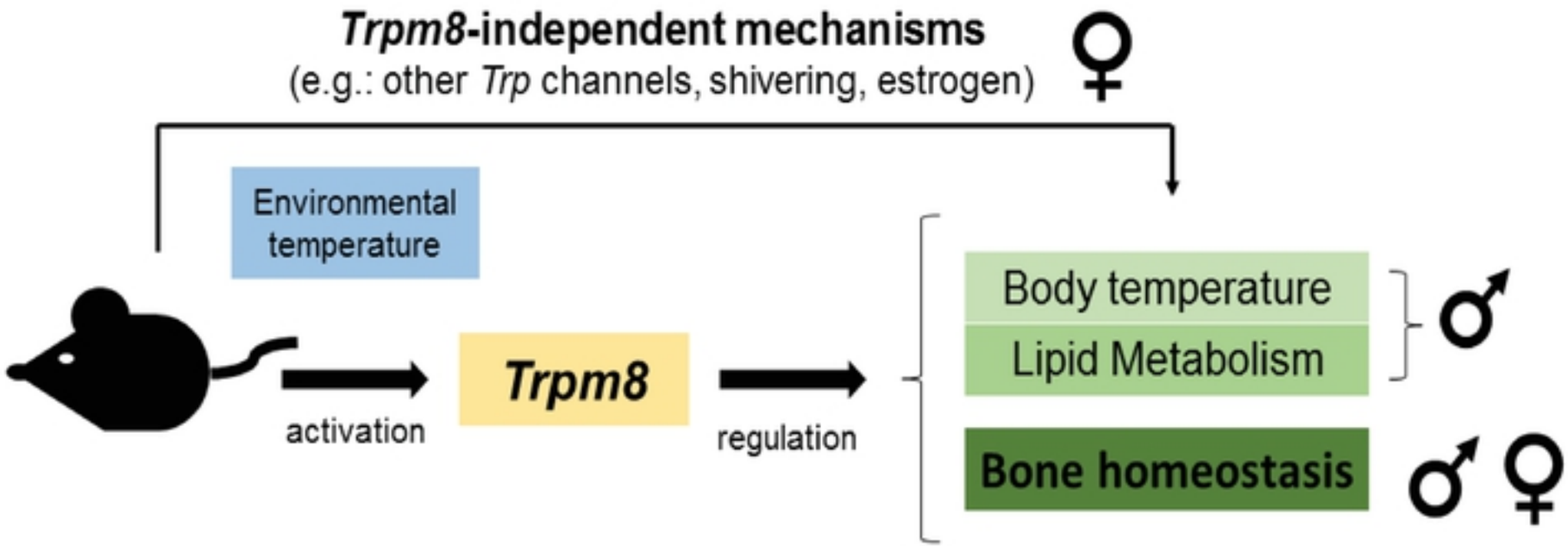

Figure 6